This article has been accepted for publication in IEEE Transactions on Signal Processing. This is the author's version which has not been fully edited and content may change prior to final publication. Citation information: DOI 10.1109/TSP.2022.3223575

Signal Useful Information Recovery by Overlapping Supports of Time-Frequency Representations

Nicoletta Saulig, Miloš Milovanović, Siniša Miličić, and Jonatan Lerga

***Abstract*—This paper presents a novel method for automatic extraction of useful information from time-frequency distributions of noisy signals. Signals' features are examined through the combined analysis of their time-frequency energy distributions and inverse complexity maps. The inverse complexity approach gives a new entropy-based insight into the signal structure. These two approaches result in mostly disjoint time-frequency supports, overlapping only in the proximity of the signal components. Locations of the signal components (i.e., useful information) are thus identified by low complexity and high amplitude occurring together in the time-frequency plane. Compared to existing methods using only the time-frequency energy distribution, useful information extraction by the proposed method exhibits a significantly reduced error rate.**

***Index Terms*—Components extraction, K-means, nonstationary signals, Rényi entropy, time-frequency distributions.**

I. Introduction

NONSTATIONARY signals are omnipresent manifestations of countless natural and artificial phenomena. Independently on the origin system being biological or physical (speech, EEG, HRV, seismic waves, gravitational waves) or synthetic (radar, sonar, vibrations in engineering), the signal of an analyst's interest is often corrupted by noise. The variable frequency content of nonstationary signals intuitively requires both the time and frequency domains simultaneously represented for a comprehensive signal interpretation, evoking time-frequency (TF) analysis tools.

In scientific and engineering disciplines, useful information content (UIC) of a signal can be framed as the entire TF content of signal components [1]. These components are compactly supported continuous energy regions, peaks of which correspond to the instantaneous frequencies (IFs) $f_l(t)$, $l = 1 \dots L$, present in the time signal [2], [3]

$$x(t) = \sum_{l=1}^{L} x_l(t) = \sum_{l=1}^{L} A_l(t) e^{j\Phi_l(t)}, \tag{1}$$

where L is the number of components, and $A_l(t)$ the instantaneous amplitude of the monocomponent signal $x_l(t)$ with IF related to instantaneous phase $\Phi_l(t)$ as $f_l(t) = \Phi_l'(t)/2\pi$.

N. Saulig is with the Faculty of Engineering, Juraj Dobrila University of Pula, Croatia. E-mail: nicoletta.saulig@unipu.hr

M. Milovanović is with the Mathematical Institute of the Serbian Academy of Sciences and Arts, Belgrade, Serbia. E-mail: milosm@turing.mi.sanu.ac.rs

S. Miličić is with the Faculty of Informatics, Juraj Dobrila University of Pula, Croatia. E-mail: sinisa.milicic@unipu.hr

J. Lerga is with the Faculty of Engineering, University of Rijeka, Croatia. E-mail: jlerga@riteh.hr

An ideal TF energy distribution (TFD), $\rho_x(t,f)$, would concentrate the signal energy along components' IFs as L components supported over 1-D trajectories,

$$\rho_x(t,f) = \sum_{l=1}^{L} A_l^2(t)\delta(f - f_l(t)). \tag{2}$$

In practice, only monocomponent signals with linear frequency modulation (FM) achieve the idealized model by the Wigner-Ville distribution (WVD). At any time t and frequency f the WVD is given by:

$$\rho_x^{\mathrm{WV}}(t,f) = \int_{-\infty}^{\infty} x\left(t+\frac{\tau}{2}\right) x^{\star}\left(t-\frac{\tau}{2}\right) e^{-j2\pi f\tau} d\tau, \tag{3}$$

with asterisk $(^{\star})$ denoting complex conjugation.

Since the WVD presents a quadratic superposition principle, general parameters of Eq. (1), including multiple components and/or nonlinear FM, cause cross-terms between any two points of components' IF [4]–[6].

The ideal TFD of Eq. (2) presents a theoretical level of sparsity [7]. A practically obtainable sparsity provides a finite and controllable bandwidth around the IF $f_l(t)$.

Realistic scenarios often include additive noise $\nu(t)$, resulting with the mixture

$$y(t) = x(t) + \nu(t). \tag{4}$$

To mitigate the interference phenomena, a quadratic class of TFDs has been introduced [1]. Discretizing the noisy model,

$$y_n = x_n + \nu_n \tag{5}$$

with $x_n = \sum_{l=1}^{L} x_{ln}, n = 1, \dots, N$ (a discretization also of Eq. (1)), quadratic class TFDs are computed as the discrete Fourier transform (DFT) of a smoothed instantaneous autocorrelation function (IAF). The smoothed IAF is obtained by the convolution of IAF with a time-lag kernel filter $G(n,i)$ (for the WVD, $G(n,i) = \delta(n)$). The TFD thus becomes [1]

$$\rho_{nm} = \underset{i\to m}{\mathrm{DFT}}\{G(n,i) \underset{n}{*} (y_{n+i}y_{n-i}^{\star})\}, \tag{6}$$

for i in an interval of integers, over M frequency bins. For $L \ll N, M$ the ideal discrete TFD is intrinsically sparse.

Often, TFD sparsity is imposed by artificially selecting TF coefficients. In numerous engineering applications, TF coefficients are thresholded by amplitude, usually as a percentage of the maximal TFD value [8]–[14]. This approach is extremely versatile, requiring no prior signal analysis or specific signal features, but the threshold choice relies on a supervised trial-and-error procedure to avoid ineffective noise suppression or severe loss of UIC.

This article has been accepted for publication in IEEE Transactions on Signal Processing. This is the author's version which has not been fully edited and content may change prior to final publication. Citation information: DOI 10.1109/TSP.2022.3223575

Methods requiring particular characteristics of the signal (such as time-invariant number or amplitude of signal components), or certain statistical features of TFDs, have been proposed for unsupervised signal UIC extraction [15]–[17]. To recover UIC from TFDs, image segmentation techniques [18]–[24] have exploited characteristic patterns of specific signals (e.g., EEG, seismic signals, speech, etc.).

Local TF entropy analysis has generated new insights into the TFD structure aimed at discriminating UIC from noise. In [25] the attempt of signal UIC extraction is based on exploiting information obtained from multiple TF entropy maps by varying the size of the 2-D entropy analysis window. However, the number of entropy maps linearly increases with the signal duration, which represents a serious limitation for the method application to real-life signals [25]. Its computational complexity is significantly reduced when an initial TFD amplitude segmentation is followed by a 1-D entropy estimate of each segment (class) while maintaining similar performance [26]. A recent study [27] presents an unsupervised method for UIC recovery, combining TFDs amplitude segmentation with a statistical criterion on the energy of each class. The method gives a single view of the signal TFD structure, and, while requiring no prior information on the signal, balances noise removal and UIC recovery. Trade-off between noise suppression and UIC integrity is inevitable when the sole TFD is used as segmentation substrate.

This paper proposes an unsupervised method that exploits the structural features of the signal TFD in relation to those of a single auxiliary TF complexity representation, namely, the newly introduced inverse complexity map (ICM) derived from 2-D entropy, to significantly reduce the presence of noise in the recovered signal. It will be shown that an auxiliary TF complexity representation, counterpart to the classical energy TFD, offers a coherent yet complementary view of the same signal, and a highly reliable identification of signal components.

The paper is structured as follows: Section II presents TF representations carrying information that may be considered complementary features of the signal, together with a criterion for relevant coefficients extraction from the TF representations. The criterion is a modification of the Intersection-of-Confidence-Intervals (ICI) algorithm which assumes knowledge on a reference set of irrelevant TF coefficients and searches for their pertinent neighbourhood. Section III analyses the relationship between obtained relevant coefficients, pointing out their statistical properties. These will be exploited in Section IV to frame representations' parameters and formulate an algorithm for UIC extraction. The algorithm's performance is evaluated in Section V. Conclusions and perspectives are reported in Section VI.

II. Relevant coefficients of different TF representations

The central theme of this paper is the extraction of the signal components to obtain a sparse representation of the signal UIC. The targeted sparse TF representation of the signal y_n is the one that recovers the non-zero coefficients laying in the TF supports of the noise-free equivalent x_n. To achieve the desired sparse TF representation of the signal UIC, a natural candidate for the application of coefficients' selection criteria is the energy TFD, ρ_{nm} [15], [17], [25]–[27]. Nevertheless, the TFD itself is characterized by local entropy features that will be shown to act as an auxiliary 2-D complexity substrate for UIC identification in the TFD. This study will show that maximization of correctly extracted UIC first requires the selection of relevant coefficients from both considered substrates. Analysis of supports of relevant coefficients of the energy TFD and 2-D complexity substrate points out their intrinsic disjointedness, except inside the supports of the signal components where they partially overlap. This last circumstance will serve as the criterion for discrimination of noise coefficients (false positives) from signal components (true-positives), allowing efficient UIC extraction from the TFD.

A. TFD and multiplicative inverse complexity map

A detailed insight into a TFD structure has been proposed through the lens of complexity measures in [28]–[31]. An appropriate measure of complexity of TFDs, especially considering negative values taken on by most TFDs, is the global Rényi entropy (RE) measure,

$$H = \frac{1}{1-\alpha}\log_2 \sum_{n,m} \overline{\rho}_{nm}^{\alpha}, \quad \overline{\rho}_{nm} = \frac{\rho_{nm}}{\sum_{n',m'} \rho_{n'm'}} \tag{7}$$

where α is the order of the RE.

The inverse complexity map (ICM) of a TFD is achieved by the reciprocal values of the locally estimated RE, as

$$H'_{nm} = (\alpha-1)\left(\log_2 \sum_{k,l} \overline{\rho}_{kl}^{\alpha}\right)^{-1}, \quad k-n, l-m \in \left[-\frac{D}{2}, \frac{D}{2}\right), \tag{8}$$

where $\overline{\rho}_{kl}$ is ρ_{kl} normalized as per Eq. (7).

Discrete TFDs, ρ_{nm}, of a pure tone, pure white Gaussian noise, and their mixture are reported in Figs. 1 (a), (e), and (i), respectively. Their ICMs, H'_{nm}, are shown in Figs. 1 (b), (f), and (j), respectively. In Figs. 1(a) and (b), the reader can observe that the TFD represents the signal as a prominent, continuous-energy cluster in the TF plane, while the ICM frames the signal component.

Ideally localized TFD concentrates the signal energy along a 1-D trajectory while finite signal windowing and time-lag filtering inevitably smear it over the TF plane. This also results in TF regions evenly covered in negligibly small coefficients exhibiting large local entropy. Large local entropy is also achieved when the window entirely slides inside the signal component support. An abrupt amplitude rise of the signal component inside the entropy window results in significantly smaller entropy values, as shown by the ICM in Fig. 1(b).

This scenario can be better observed from concurrently represented time cross-sections of the TFD (blue, solid) and ICM (green, solid) in Fig. 1(d). The instant when the entropy window (marked by a double arrow) catches brusquely growing TFD coefficients corresponds to an abrupt inverse complexity rise. Appropriate entropy window selection is discussed in Section IV-A2.

This article has been accepted for publication in IEEE Transactions on Signal Processing. This is the author's version which has not been fully edited and content may change prior to final publication. Citation information: DOI 10.1109/TSP.2022.3223575

B. Maps of relevant coefficients

The case of both representations of noise-free signals (Figs. 1(a), and (b)) can be perceived as theoretically sparse in the TF domain. However, the smearing effects of the kernel filter produce what we consider practical sparsity of these components and frames. Presence of noise (Figs. 1(i), and (j)) obstructs desired sparsity.

Aiming to obtain a sparse representation of the signal UIC from the TFD, the approach proposed in this work is based on a preselection of specific coefficients subsets from both the TFD and ICM. These will be referred to as relevant coefficients. A relevant coefficient is discriminated from a background one, for both the TFD and ICM, by a data-driven, automatically computed threshold, as follows. Selection of relevant coefficients from a general matrix f_{nm} is performed by amplitude discrimination computed by the K-means algorithm [32].

The K-means algorithm partitions a matrix f_{nm} with $n = 1,\dots,N$ and $m = 1,\dots,M$, into K subsets of indices $\mathcal{C} = \{C_1,\dots,C_K\}$, in order to minimize the within-subset sum of squares,

$$\underset{\mathcal{C}}{\operatorname{argmin}} \sum_{k=1}^{K} \sum_{(n,m)\in C_k} \|f_{nm} - \mu_k\|^2, \tag{9}$$

where μ_k is the mean of each set C_k, and the values of μ_k are strictly increasing with respect to k. Thus, K classes (matrices) $f_{nm}^{(1)},\dots f_{nm}^{(K)}$, derived form the function f_{nm}, are obtained as

$$f_{nm}^{(k)} = \begin{cases} f_{nm}, & \text{where } (n,m) \in C_k \\ 0, & \text{elsewhere.} \end{cases} \tag{10}$$

Both the TFD, ρ_{nm}, and ICM, H'_{nm}, taking place as argument of Exp. (9) can be partitioned into K classes. However, the partitioned set $\mathcal{C}$ gives no *a priori* information about which classes C_k contain the relevant coefficients.

Signals' components (in the TFD) and their frames (in the ICM) both consist of sharp ridges plotting trajectories in the TF plane. It is, hence, reasonable to expect that classes containing mainly background coefficients will present significantly larger TF supports when compared to classes containing relevant coefficients.

We apply a statistical method [27] adapted to discriminate background from relevant classes by means of their TF supports. Since both the TFD, ρ_{nm}, and ICM, H'_{nm}, are partitioned into K classes, a common model will be adopted for both representations, and again generically denoted as f_{nm}.

The size of the TF support, or l_0-norm, of the k-th class is the cardinality of the respective set C_k,

$$E_k = \operatorname{card} C_k. \tag{11}$$

We use the values of E_k as input for a threshold to distinguish two subsets of $\mathcal{C}$, such that $\mathcal{C} = \mathcal{C}_b \cup \mathcal{C}_r$, with

$$\mathcal{C}_b = \{C_k | \, k = 1,\dots i^+\}, \quad \mathcal{C}_r = \mathcal{C}\backslash\mathcal{C}_b, \tag{12}$$

where $\mathcal{C}_b$ contains the background coefficients, and the subset $\mathcal{C}_r$ the relevant ones. In that sense, the class index $k = i^+ + 1$ marks the first class containing relevant information.

To obtain the class index i^+, we estimate the pertinent neighborhood of E_1.

By relying on the assumptions that signal components and their frames represent the amplitude-wise dominant structures on the TF plane, we expect the first (lowest) class, $f_{nm}^{(1)}$, for both representations to contain mainly noise and residual components' coefficients smeared by filtering. Labeling the first class, $f_{nm}^{(1)}$, as background on theoretical grounds reduces computational burden by K times when compared to the original Intersection-of-Confidence-Intervals (ICI) method in [33]–[35].

Using the first class, $f_{nm}^{(1)}$, as the background reference class, its neighborhood now represents the background classes, while distant classes are the relevant part.

To determine the neighborhood of $f_{nm}^{(1)}$ by estimating the neighborhood of E_1, we introduce confidence intervals Δ_i around the corresponding $\hat{E}_i$ estimate of an ideal value $\tilde{E}_1$, with indices $i = 1,\dots,K$ and

$$\hat{E}_i = \frac{1}{i}\sum_{k=1}^{i} E_k. \tag{13}$$

The ideal $\tilde{E}_1$ is considered to be the l_0-norm of the first class as the result of an ideal, flawless segmentation of f_{nm}. We define i^+ as the largest index such that

$$\bigcap_{i=1}^{i^+} \Delta_i \neq \varnothing, \tag{14}$$

and the estimation error $e_i = \tilde{E}_1 - \hat{E}_i$ is minimal [36].

The estimation error for a class is composed of bias and zero-mean random error [33],

$$e_i = \omega_i + \zeta_i^0, \tag{15}$$

where ω_i the estimation bias [33], and, hence, its absolute value can be bounded by

$$|e_i| \leq |\bar{\omega}_i| + |\zeta_i^0|, \tag{16}$$

where $\bar{\omega}_i$ is the estimation error bias upper limit and ζ_i^0 is the random error following the zero mean normal Gaussian distribution with standard deviation σ_i, equivalently $\zeta_i^0 \sim \mathcal{N}(0,\sigma_i^2)$. The following inequality holds true with probability $1-a$,

$$|\zeta_i^0| \leq z_{1-a/2}\sigma_i, \tag{17}$$

where z_α is the α-th quantile of the unit normal distribution $\mathcal{N}(0,1)$ [33], [34]. Hence, Ineq. (16) can be rewritten as

$$|e_i| \leq |\bar{\omega}_i| + z_{1-a/2}\sigma_i, \tag{18}$$

and it also holds true with the same probability of $1-a$.

The inequality

$$|\bar{\omega}_i| \leq \gamma\sigma_i, \tag{19}$$

where γ is defined in [33] as the ratio of the upper-bound bias to the standard deviation for an ideal i^* is true for all $i < i^*$. Setting $\Gamma = \gamma + z_{1-a/2}$ in Ineq. (18),

$$|e_i| = |\hat{E}_i - \tilde{E}_1| \leq \Gamma\sigma_i, \tag{20}$$

which holds with same probability $1-a$. For very small a, the critical threshold may not exist at all, and for very large a,

This article has been accepted for publication in IEEE Transactions on Signal Processing. This is the author's version which has not been fully edited and content may change prior to final publication. Citation information: DOI 10.1109/TSP.2022.3223575

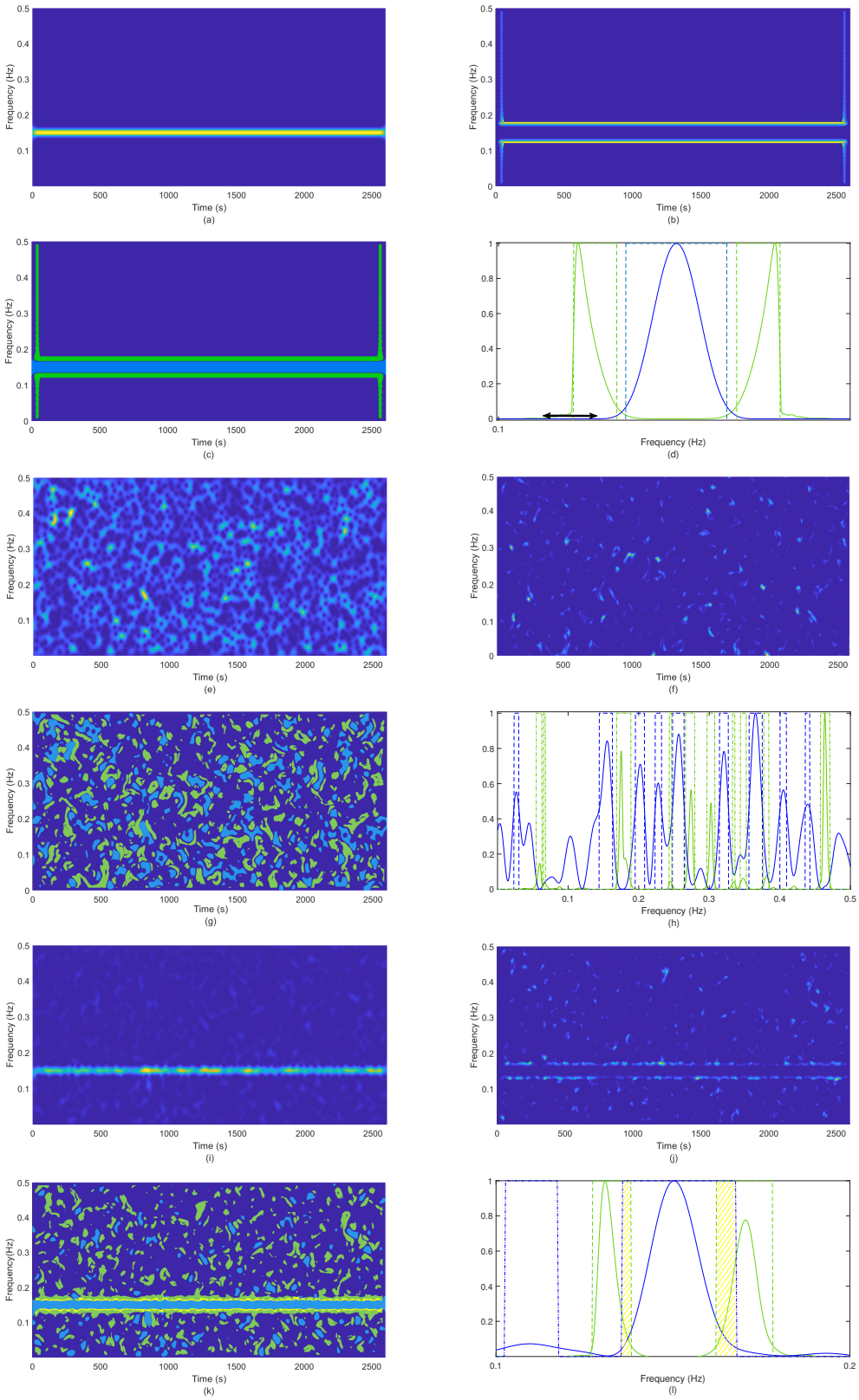

Fig. 1: TFDs (spectrograms) of the signals (a), (e), (i). ICMs of the signal (b), (f), (j). Supports of relevant coefficients of the TFD (azure), ICM (green), their overlapping (yellow) (c), (g), (k). Cross-sections (t = 1600 s) of the TFD and ICM (azure for the TFD, green for the ICM) and respective supports of relevant coefficients (dashed), with overlappings marked yellow (d), (h), (l). Signals are referred to as a pure tone (a)-(d), pure white Gaussian noise (e)-(h), and a noisy pure tone (SNR = $2dB$) (i)-(l).

This article has been accepted for publication in IEEE Transactions on Signal Processing. This is the author's version which has not been fully edited and content may change prior to final publication. Citation information: DOI 10.1109/TSP.2022.3223575

the threshold may be too low. Following [27] we set $\Gamma = 0.65$, corresponding to $a \approx 50\%$.

In other words, it can be said that the ideal $\tilde{E}_1$ belongs to the interval

$$\Delta_i = [\hat{E}_i - \Gamma\sigma_i, \hat{E}_i + \Gamma\sigma_i]. \tag{21}$$

with the probability $1 - a$.

Finally, the class index i^+ is obtained in Ineq. (14) as the largest one for which it is still true that the intersection of all confidence intervals up to, and including i^+, is nonempty.

The index i^+ can be considered as an approximation of the ideal one i^*, resulting in an estimation of $\hat{E}_{i^+}$ as close as possible to the optimal $\hat{E}_{i^*}$.

By adopting the first class as background, all the non-zero coefficients belonging to the subsets for which $k \leq i^+$ form $\mathcal{C}_b$. In other words, the remaining classes are summed up to recover relevant information as

$$f_{nm}^R = \sum_{k=i^++1}^{K} f_{nm}^{(k)}. \tag{22}$$

Using this method we obtain the relevant TF coefficients ρ_{nm}^R from ρ_{nm}, and relevant ICM coefficients $H_{nm}^{\prime R}$ from $H_{nm}^{\prime}$. Where their indices are not relevant, we will omit them.

III. Relations between relevant coefficients of the TFD and ICM

Once relevant coefficients have been selected from both the TFD, ρ^R, and ICM, $H^{\prime R}$, to improve UIC extraction, their arrangement, relationship and its stability over the TF plane will be analyzed for three characteristic situations: noise-free signal, pure noise, and noisy signal.

In this analysis we denote as $\rho^{\overline{R}}$ and $H^{\prime\overline{R}}$, $0-1$ valued supports of relevant coefficients ρ^R and $H^{\prime R}$, respectively. Examples of $\rho^{\overline{R}}$ and $H^{\prime\overline{R}}$, are shown in Figs. 1(c), (g), and (k), for the noise-free pure tone, pure noise, and noisy pure tone, respectively.

A. Noise-free signal

By analyzing the supports of relevant coefficients for the noise-free signal (Fig. 1(c)) it can be observed that $H^{\prime\overline{R}}$ (green) will act as an edge detector for $\rho^{\overline{R}}$ (azure). We also observe some artifacts near the edges of the domain, but since these do not appear in the analysis of the noisy signal, we shall disregard them.

A careful analysis of a time cross-section of the TFD and ICM reveals that the latter peaks (Fig. 1(d), green solid line) are distributed on both sides of the TFD energy ridge. If we observe the supports of relevant coefficients $H^{\prime\overline{R}}$ and $\rho^{\overline{R}}$ (Fig. 1(d), dashed lines), they can be considered disjoint indeed. In fact, relevant coefficients present mutually exclusive supports, as marked by the dashed lines in Fig. 1(d).

B. Gaussian white noise

To see if the two approaches we combine here obtain dependent, yet different information, we investigate whether for pure Gaussian white noise we obtain probabilistically dependent, almost-disjoint results.

TABLE I: Sample means and standard deviations for correlations and PMI computations for Gaussian white noise and reference data. Samples were of size 100 each.

	mean		standard deviation	
$\overline{\rho^{\overline{R}}}$		$1.3 \cdot 10^{-1}$		$3.5 \cdot 10^{-2}$
$\overline{H^{\prime\overline{R}}}$		$1.4 \cdot 10^{-1}$		$1.5 \cdot 10^{-1}$
$\overline{H^{\prime\overline{R}} \odot \rho^{\overline{R}}}$		$9.4 \cdot 10^{-5}$		$1.5 \cdot 10^{-4}$
$\mathrm{PMI}(\rho^{\overline{R}}, H^{\prime\overline{R}})$	μ_p	$-6.8 \cdot 10^{0}$	σ_p	$2.1 \cdot 10^{0}$
$\mathrm{PMI}(\rho_0, H_0^{\prime})$	μ_{p0}	$-5.5 \cdot 10^{-3}$	σ_{p0}	$9.1 \cdot 10^{-2}$

We do this by sampling pure noise and investigating the relationships between supports of relevant coefficients $\rho^{\overline{R}}$ and $H^{\prime\overline{R}}$. An analysis of a single sample is given in Figs. 1(g) and (h). Figure 1(g) shows the TF supports of relevant coefficients $\rho^{\overline{R}}$ and $H^{\prime\overline{R}}$ (azure and green patches) are rarely overlapping. Figure 1(h) shows one time cross-section, with supports of relevant coefficients marked by dashed lines.

These properties are best quantified using measures of independence, for which we use point-wise mutual information (PMI). For a method to provide mostly disjoint results, we expect the measure to show significant negativity. As a result, we find significant deviations from independence in the direction of disjointness.

For reference, we compute the PMI for random pairs of energy distributions of pure Gaussian noises, filtered through the branches of the algorithm. The first branch goes through the ICI pipeline to obtain $\rho^{\overline{R}}$, and the second through the ICM and ICI for $H^{\prime\overline{R}}$.

The PMI analysis is performed as follows. First, we compute $\mathrm{PMI}(H^{\prime\overline{R}}, \rho^{\overline{R}})$ using

$$\mathrm{PMI}(x, y) = \ln\left(\frac{\overline{x \odot y}}{\overline{x} \cdot \overline{y}}\right), \tag{23}$$

where $\odot$ refers to the element-wise (Hadamard) matrix product, and $\overline{(.)}$ is the average across the whole matrix. We also compute the PMI for pairs of matrices in a reference set.

Since we have some non-overlapping pairs of supports in our sample, producing negative infinities, we clamp the infinite data points to the finite minimum of the PMI sample. This reduces the standard deviation, but the mean becomes informatively finite.

For values of $\mathrm{PMI}(H^{\prime\overline{R}}, \rho^{\overline{R}})$, we obtain mean of $\mu_p = -6.8$ with $\sigma_p = 2.1$ and maximum at -3.77. The reference set gives us $\mu_{p0} = -0.0055$ with $\sigma_{p0} = 0.091$. A histogram of the data is shown in Fig. 2. Thus, using the standard deviation of the reference set as a reasonable unit, even the maximum is 42 standard deviations away from independence, in the (negative) direction of disjointness.

The results, along with data on the intersections and support sizes, are reported in Table I, with $H_0^{\prime}$ and ρ_0 denoting supports of reference set pairs.

In conclusion, the preponderance of numerical evidence of mutual dependence of $H^{\prime\overline{R}}$ and $\rho^{\overline{R}}$, indicates pure noise supports can be considered, from a practical point of view, disjoint in the TF plane.

This article has been accepted for publication in IEEE Transactions on Signal Processing. This is the author's version which has not been fully edited and content may change prior to final publication. Citation information: DOI 10.1109/TSP.2022.3223575

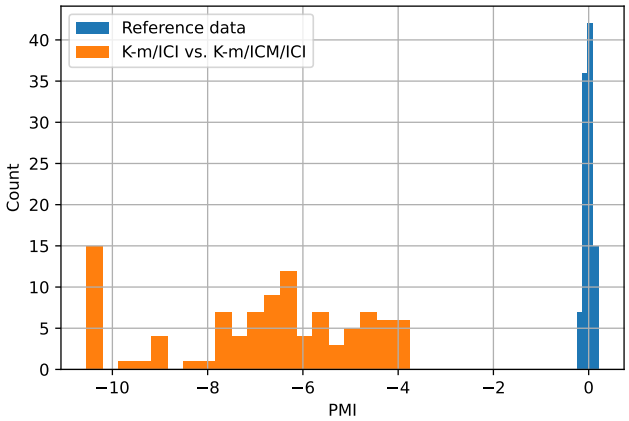

Fig. 2: PMI data histogram for Gaussian white noise analysis.

C. Noisy signal

So far, the supports of relevant TFD and ICM coefficients have been considered for each summand of Eq. (5) separately. However, when their sum is considered, the ICI-based algorithm produces supports reported in Fig. 1(k).

Figure 1(l), presenting a time-instant cross-section of both the TFD and the ICM, shows that the supports of relevant coefficients are again mutually exclusive in the regions of the TF plane not occupied by the signal component, while in its proximity they largely overlap (yellow regions mark the overlappings of $\rho^{\overline{R}}$ (azure dashed lines), and $H'^{\overline{R}}$ (green dashed lines)). This can be explained by the intrinsic structural characteristics of the noisy signal TFD and its relationship with the ICM.

Noise in TFDs has been extensively studied. The structure of the Wigner distribution (WD), defined by the kernel in the discrete time-lag domain $G(n,i)=\delta(n)$, has been studied for stochastic processes and deterministic signals in random noise [37]. The WD produces white noise power spectrum estimates of infinite variance [37], [38].

White Gaussian noise is evenly distributed over the TF plane, i.e., an additive white noise model can be adopted in the case of the WD, while the TFD kernel determines the variance finite value if the TFD is computed over a finite number of data samples [38]–[42].

A detailed insight into the structure of a discrete-time quadratic TFD of a noisy signal requires the definition of the quadratic class distribution of ν_n, (as per [43])

$$\rho^{G}_{\nu,nm}=\sum_{q,i}G(q,i)\nu_{n+q+i}\nu^{\star}_{n+q-i}e^{-j4\pi mi}, \tag{24}$$

where $G(q,i)$ is the kernel in the time-lag domain.
For stationary white noise, as shown in [43] the maximum of the variance $\sigma^2_{\nu\nu}$ of ρ^{G}_{ν} is proportional to kernel's energy,

$$\max\sigma^2_{\nu\nu,nm}=2\sigma^4_{\nu}\sum_{q,i}|G(q,i)|^2\propto\sigma^4_{\nu}, \tag{25}$$

with σ^2_{ν} being the noise variance.

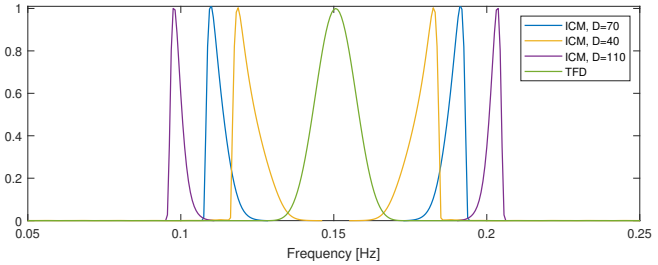

Fig. 3: Time cross-section of the TFD and ICM for different values of entropy window size D.

For the deterministic signal x corrupted by noise, $y=x+\nu$, however, the TFD variance σ^2_{ρ} consists of two components [41], [42]

$$\sigma^2_{\rho,nm}=\sigma^2_{\nu\nu,nm}+\sigma^2_{x\nu,nm}. \tag{26}$$

The first variance component, $\sigma^2_{\nu\nu}$, is bounded by the energy of the kernel as per Eq. (25), while for analysis of the second, signal-dependent component $\sigma^2_{x\nu}$, we will consider the inner product form of the quadratic class of distributions

$$\rho^{\tilde{G}}_{y,nm}=\sum_{i,q}\tilde{G}(q,i)(y_{n+q}e^{-j2\pi mq})(y_{n+i}e^{-j2\pi mi})^{\star}, \tag{27}$$

where $\tilde{G}(q,i)=G\left(\frac{1}{2}(q+i),\frac{1}{2}(q-i)\right)$. For real and symmetric $G(q,i)$ we get [43]

$$\sigma^2_{x\nu,nm}=2\sum_{\eta,\xi}\tilde{\Phi}(\eta,\xi)(x_{n+\eta}e^{-j2\pi m\eta})(x_{n+\xi}e^{-j2\pi m\xi})^{\star}, \tag{28}$$

where the new kernel is given by

$$\tilde{\Phi}(\eta,\xi)=\sum_{i_1,i_2}\tilde{G}(\eta,i_1)\tilde{G}^{\star}(\xi,i_2)e^{-j2\pi m(i_2-i_1)}R_{\nu,n+i_2,n+i_1}, \tag{29}$$

with R_{ν} being the noise autocorrelation function.

Thus, as shown in [43], we have that, lacking strong noise autocorrelations, the signal-dependent part of the variance σ^2_{ρ} is again of the form of the quadratic TFD of the deterministic signal x,

$$\sigma^2_{x\nu,nm}=2\rho^{\tilde{\Phi}}_{x,nm}. \tag{30}$$

The ICM emphasizes small entropy values. Large entropy is achieved within windows of relatively flat content, and is significantly reduced where variance is large.

Signal-shaped variance of Eq. (30) in presence of noise distorts complexity in the vicinity of UIC. This complexity, emphasized by the ICM, generously superimposes over prominent amplitudes of the TFD. Consequently, supports of relevant coefficients of both $\rho^{\overline{R}}$ and $H'^{\overline{R}}$ noticeably overlap. This scenario is shown in Figs. 1(k) and (l).

IV. Parametrization and the Algorithm for Useful Information Extraction

This section addresses proper parameter selection for the two TF representations to assure overlapping of the respective relevant coefficients along components borders and disjointness elsewhere. We also present the algorithm for the extraction of the UIC, by removal of noise-generated/false-positive coefficients.

This article has been accepted for publication in IEEE Transactions on Signal Processing. This is the author's version which has not been fully edited and content may change prior to final publication. Citation information: DOI 10.1109/TSP.2022.3223575

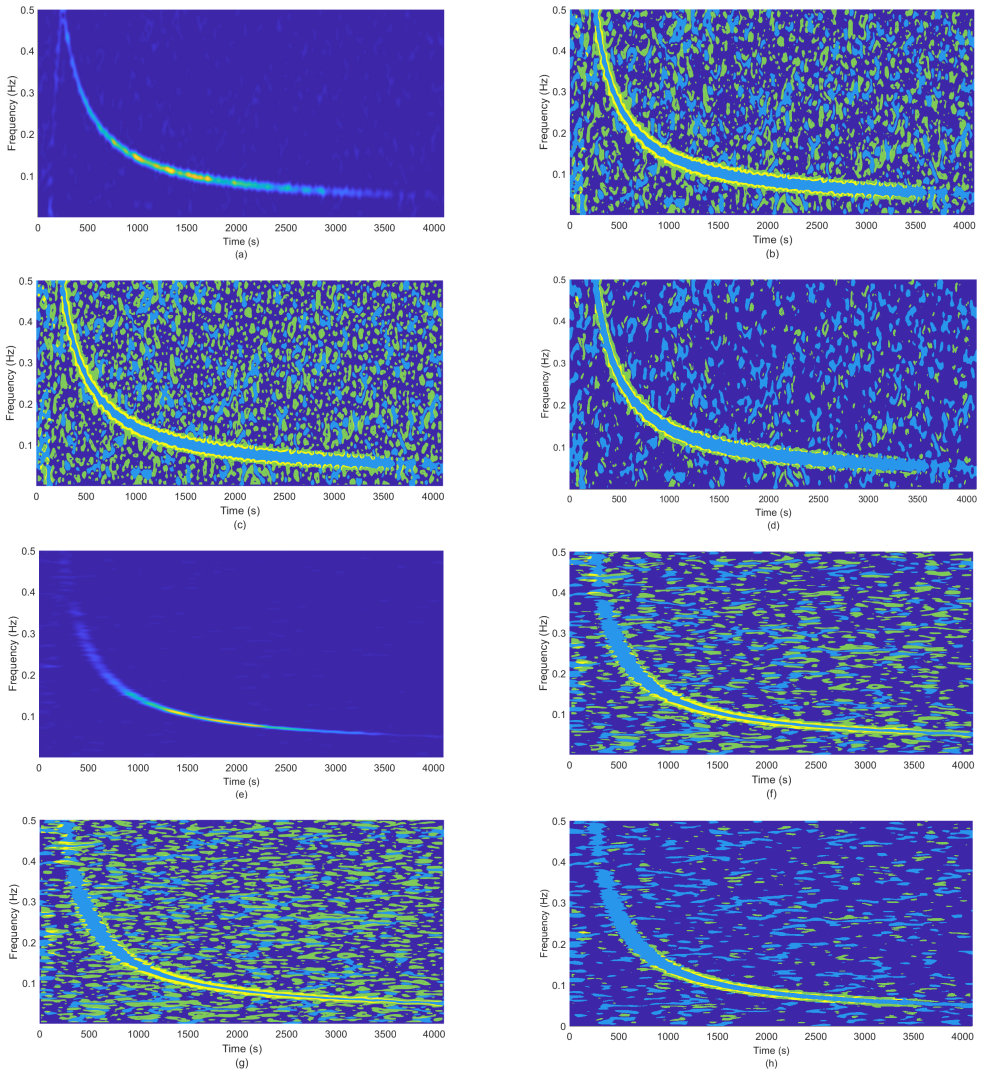

Fig. 4: Noisy spectrograms (AWGN, SNR = 2 dB) with *Hamming* window of length W = 85 (a), and *Hamming* window of length W = 285 (e). Supports of relevant coefficients obtained for: D = 46 (b), (f); D = 36 (c), (g); D = 56 (d), (h).

A. Parameter tuning

1) The entropy order α: The order α of the RE nonlinearly dissociates nonuniform distributions from uniform ones. The ICM always has uniform distributions as minima. Large α can become numerically unstable, while small α identifies mild edges that are likely to be originating from noise. Thus, α being 7 represents the least value of α that balances both of these issues.

2) Size of the entropy window D: The ICM structure is determined by the size of the entropy window D. In fact, H' acts like a frame regarding TF energy structures, since the local complexity drop is triggered by sudden amplitude changes of ρ in the vicinity of prominent structures. In the illustrative case of a pure tone (f_0 = 0.15 Hz), for which Fig. 3 reports TFD and ICM time cross-sections, it can be observed that the distance of the ICM peaks from the TFD dominant peak is proportional to the size of the entropy window D, with faster expiring of complexity changes as D increases. The parameter D influences H', and therefore also the support of relevant coefficients $H'^{\overline{R}}$.

Figure 4 shows the influence of the parameter D on $H'^{\overline{R}}$ for a signal with hyperbolic FM. The proposed example is displayed for two spectrogram realizations of the noisy signal, with different kernel parameters (Figs. 4(a), (e)).

Desired overlapping of the respective relevant coefficients $H'^{\overline{R}}$ (green) and $\rho^{\overline{R}}$ (azure), i.e. $H'^{\overline{R}} \odot \rho^{\overline{R}}$ (yellow), along components borders and disjointness elsewhere is favored by approximately equal total supports of the Hadamard product factors, which is controlled by the size of the entropy window D (in Fig. 4 achieved for D = 46 (b), (f)). In the extremes, as previously introduced by Fig. 3, setting D too low results in ICM producing slowly varying values. As a result, ICI will produce $H'^{\overline{R}}$ having many noise-induced points as relevant. Analogously, setting D too large pushes the threshold for abrupt changes too high, potentially ignoring the edges of signal components.

To balance the value of D we observe the resulting value of $\overline{H'^{\overline{R}}}$, with $\overline{(.)}$ denoting the average across the whole matrix.

This article has been accepted for publication in IEEE Transactions on Signal Processing. This is the author's version which has not been fully edited and content may change prior to final publication. Citation information: DOI 10.1109/TSP.2022.3223575

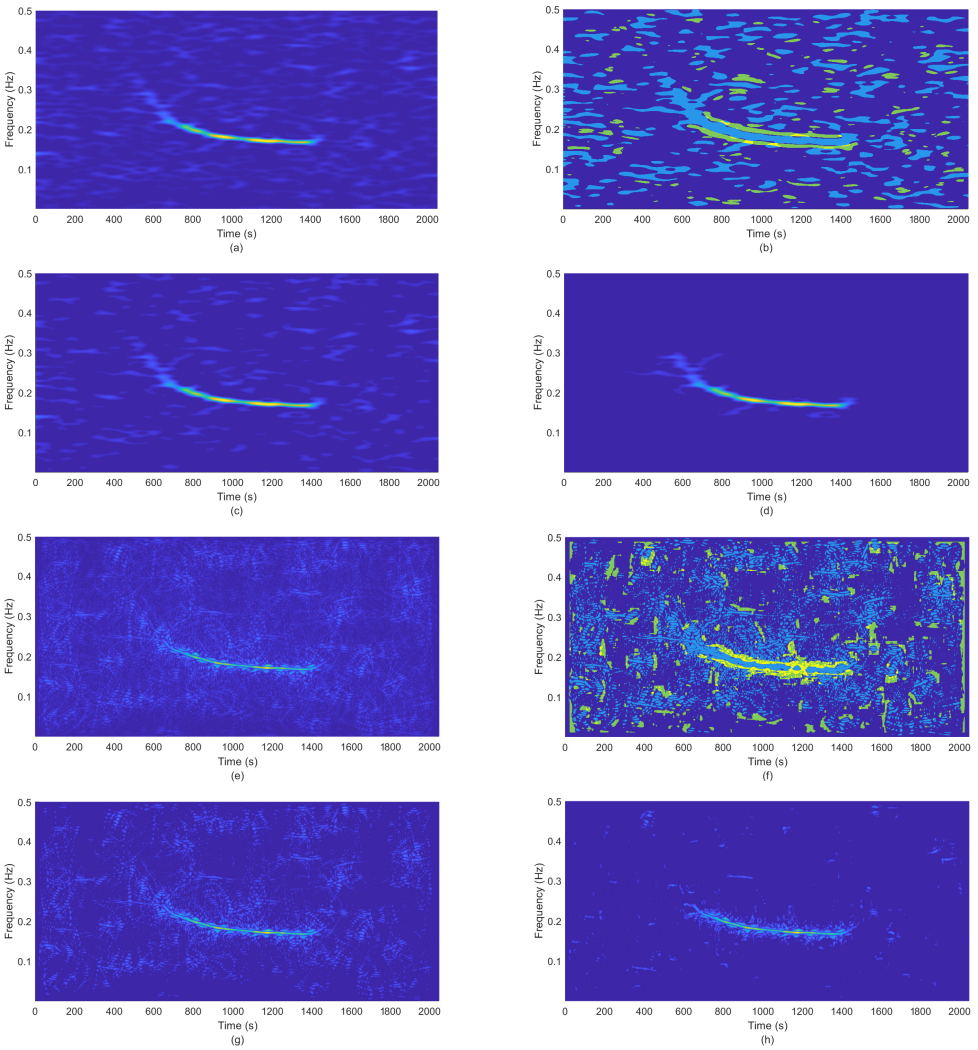

Fig. 5: Noisy TFD of a real-life bat sonar signal (a), (e). Supports of relevant coefficients (b), (f). Information extracted by the K-means/ICI algorithm (c), (g). Information extracted by the proposed method (d), (h). TFDs are referred to as SPWVD with time and lag *Hamming* windows of length $W = 115$ (a)-(d), and ZAM with *Hamming* window of length $W = 205$, $a = 3$ (e)-(h).

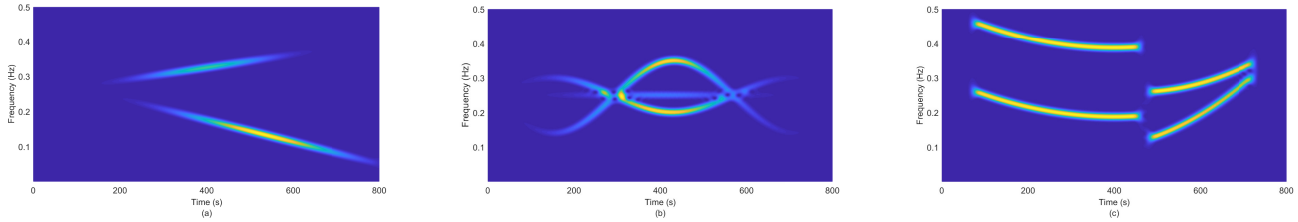

Fig. 6: Spectrograms of noise-free test signals, referred to as *Sig1* (a), *Sig2* (b), and *Sig3* (c).

We measure it against the size of the relevant TFD coefficients, minimizing $||\overline{H}'^{\overline{R}} - \overline{\rho}^{\overline{R}}||_1$, where only $\overline{H}'^{\overline{R}}$ depends on the choice of D.

To achieve a slow-moving dependence on the duration of the signal N, we seek D as

$$D(a,b) = 2\lfloor a \ln N + b \rfloor, \tag{31}$$

where $\lfloor x \rfloor$ denotes the largest integer less than or equal to x, ensuring D is even.

We obtain the values of a and b by minimizing over a wide range of test signals with N ranging from 2^7 to 2^{16}:

$$||\overline{H}'^{\overline{R}} - \overline{\rho}^{\overline{R}}||_1, \tag{32}$$

with $\overline{H}'^{\overline{R}}$ depending on a and b through D, resulting in $a = 1.9$ and $b = 8.1$.

Thus, we have identified the parameters needed for ICM that work well for various TF kernels and their parameters.

This article has been accepted for publication in IEEE Transactions on Signal Processing. This is the author's version which has not been fully edited and content may change prior to final publication. Citation information: DOI 10.1109/TSP.2022.3223575

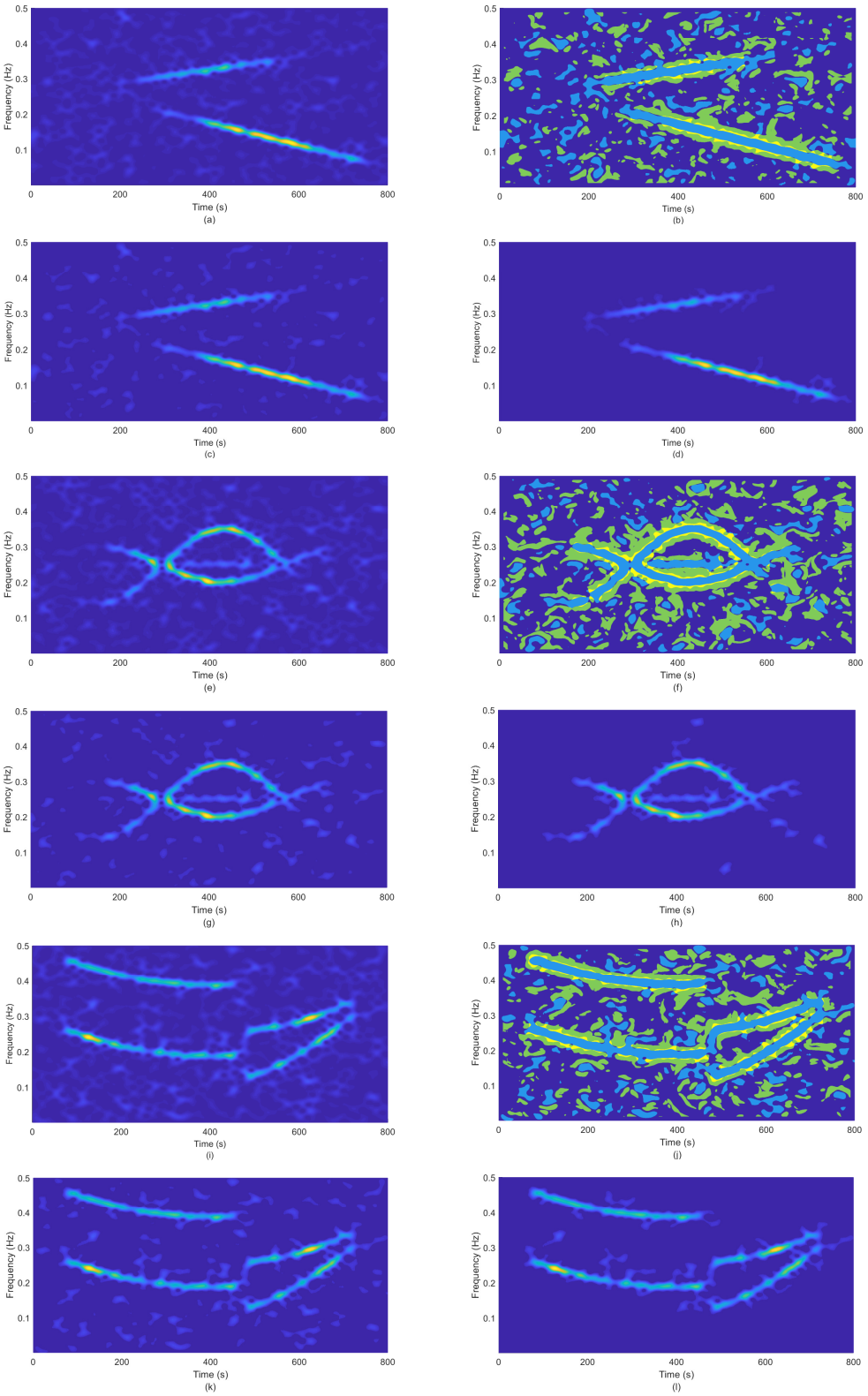

Fig. 7: Noisy spectrograms (AWGN, $\mathrm{SNR} = 0\,dB$) (a), (e), (i). Supports of relevant coefficients (b), (f), (j). Information extracted by the K-means/ICI algorithm (c), (g), (k). Information extracted by the proposed method (d), (h), (l). Signals are referred to as *Sig1* (a)-(d), *Sig2* (e)-(h), and *Sig3* (i)-(l).

This article has been accepted for publication in IEEE Transactions on Signal Processing. This is the author's version which has not been fully edited and content may change prior to final publication. Citation information: DOI 10.1109/TSP.2022.3223575

It is worth noting that Eq. (31) should be intended as a rather loose parameter constraint since desirable features of the ICM are maintained over a wide range of values around the one determined by minimizing Exp. (32), as shown by the results of varying D by 20%, negatively in Figs. 4(c), (g), and positively in Figs. 4(d), and (h).

Thus, the choice of D cannot be considered critical in parameter tuning.

3) The number of classes K: The K-means segmentation procedure requires the number of classes K as an input parameter. Since the ICM structure is intrinsically related to the TFD, the same number of classes K is chosen for their segmentation.

The purpose of the segmentation procedure consists in producing classes exhibiting characteristic supports' features of noise in contraposition to those of signal components. The parameter K determines the refinement degree of data classification, influencing the algorithm's performance, but also the computational complexity. In these terms, carrying thrift to extremes with only a few classes imposes unwanted rough partitioning of the input data. Conversely, besides increasing the computational burden, pushing K towards large values thins down the ability of the ICI algorithm to delimit a firm cutoff between noise classes and those supporting relevant information. This results in an abundance of residual noise-generated coefficients in classes identified as carriers of relevant information. Thus, while maintaining K in the band of moderate values suggested in [44], where the influence of K has been studied for TFD segmentation in 1-D entropy based UIC extraction [26], the choice of K for K-means clustering is marginal. Results for different values of K are reported and commented on in Section V.

B. Algorithm implementation

With the aim of recovering the UIC of the signal, we propose an algorithm whose output is the extracted information ρ^{EI}, given by districts of supports of relevant TF coefficients $\rho^{\overline{R}}$ intersecting the relevant ICM coefficients' supports, $H'^{\overline{R}}$. The algorithm pseudo-code is given in Algorithm 1.

A district is defined as a labeled 8-connected region of constant value [45]. The function $\mathrm{bwlabel}$ labels districts of the argument matrix as integers starting from 1. Conversely, $\mathrm{getlabel}(B, i)$ returns the support of district labeled as i in B as a matrix of values 0 or 1.

In the pseudo-code we use the following point-wise operations. Operation $\odot$ represents the Hadamard product of matrices, operation $|$ represents the bit-wise OR, and $\max$ is the maximum.

To initialize the mask matrix, $\mathrm{zerosLike}$ gives a matrix of zeros of the same form as the argument.

An edge-case occurs when the noise level is very low or negligible. We identify that case by the class index i^+ for TFD coefficients being equal 1, with i^+ defined in Section II-B. In that case, we may have disjoint districts of ρ^R and H'^R of useful information, as expected per discussion in Section III-A. So, if i^+ equals 1 and the size of the support of ρ^{EI} (denoted $\overline{\rho}^{\overline{\mathrm{EI}}}$) falls below a threshold fraction of $\overline{\rho}^{\overline{R}}$, i.e. the size of the support of ρ^R, we accept ρ^R as the final output rather than ρ^{EI}. As a threshold parameter for results reported in this paper we use 70%.

Notwithstanding the noise free edge-case, the full process introduced in this paper is thus:

1) compute ρ^R by ICI
2) compute H'^R by ICM and ICI
3) apply Algorithm 1 to ρ^R and H'^R to obtain ρ^{EI}.

Algorithm 1: Pseudo-code for computing the extracted information ρ^{EI} given H'^R and ρ^R.

```
Result: ρ^EI
A := H'^R ⊙ ρ^R̄;
B := bwlabel(ρ^R̄);
mask := zerosLike(ρ^R);
for i = 1, ..., max(B) do
    B' := getlabel(B, i);
    if max(B' ⊙ A) ≠ 0 then
        mask := mask|B';
    end
end
ρ^EI := mask ⊙ ρ^R
```

Since we use a K-means clustering algorithm with a parametrized number of iterations I, the computational complexity for step 1 is $O(N^2 I_{\mathrm{ICI}} K)$, for step 2 $O(N^2 I_{\mathrm{ICM}} K) + O(N^2 \ln^2 N)$, and for step 3, $O(\delta N^2)$ with δ representing the number of districts. Thus, the computational complexity is

$$O\left(N^2\left(I_{\mathrm{ICM}}K + I_{\mathrm{ICI}}K + \ln^2 N + \delta\right)\right). \tag{33}$$

We control the values of K, I_{ICI} and I_{ICM}, while N is the number of signal samples. The theoretical worst-case scenario for δ is $o(N^2)$, but in practice $\delta \ll N$. Thus, complexity is largely driven by N^2, just like in [27].
For example, algorithms based on full 2-D entropy computation [25] have the complexity of order N^5 as a consequence of dense sampling of entropy windows.

V. Results on real and synthetic data

The strength of the presented approach consists in the significant suppression of noise from relevant TF coefficients ρ^R, allowed by completing information derived from the ICM relevant coefficients H'^R. Based on their characteristic steps, the existing approach that provides ρ^R as extracted information [27], and the proposed one, will be referred to as K-m/ICI, and K-m/ICI/ICM, respectively.

Figure 5 is concerned with comparison of the K-m/ICI and K-m/ICI/ICM performances for real-life data, namely a bat sonar signal, recorded with a sampling frequency of 230.4 kHz and an effective bandwidth of [8 kHz, 80 kHz][1]. To confirm the K-m/ICI/ICM method's versatility, results are computed for two exponents of the well-performing quadratic class TFDs, namely the Smoothed Pseudo WVD (SPWVD), and the Zhao-Atlas-Marks (ZAM) distribution [1]. The noisy TFDs

[1]This recording was part of the research program RCP 445 supported by CNRS (Centre National de la Recherche Scientifique, France), [46].

This article has been accepted for publication in IEEE Transactions on Signal Processing. This is the author's version which has not been fully edited and content may change prior to final publication. Citation information: DOI 10.1109/TSP.2022.3223575

are reported in Figs. 5(a), and (e). The supports of relevant coefficients $H'^{\overline{R}}$ and $\rho^{\overline{R}}$ are reported in Figs. 5(b), and (f). Extracted information is reported in Figs. 5(c), and (g) for the K-m/ICI method, while the proposed K-m/ICI/ICM approach achieves results shown in Figs. 5(d), and (h).

For real data, lacking a noise-free signal counterpart needed for objective performance evaluation, the visual assessment suggests the superiority of the method when compared to the K-m/ICI approach. That needs to be confirmed by numerical evidence on synthetic data.

To validate the performance of the proposed algorithm three synthetic signals are considered, referred to as $Sig\,1$, $Sig\,2$, and $Sig\,3$; the sparse signals' TFDs are reported in Figs. 6(a), (b), and (c), respectively. TFDs of their noisy equivalents are shown in Figs. 7(a), (e), and (i). Signals' analytic forms and parameters are reported in Table II.

Each of the three test signals consists of multiple components with different FM. In the case of $Sig\,2$ the signal components overlap in the TF plane. However, the UIC is intended as a whole, setting aside whether its structure is characterized by well separated components or overlapping ones. Thus, lack of components' separability is not an impediment for the method performance.

The supports of relevant coefficients $H'^{\overline{R}}$ and $\rho^{\overline{R}}$ are reported in Figs. 7(b), (f), and (j).

The extracted information is reported in Figs. 7(c), (g), and (k) for the K-m/ICI method, in comparison to the results provided by the K-m/ICI/ICM method and shown in Figs. 7(d), (h), and (l). Visual evaluation of the results obtained by the compared methods reveals the impression of significantly better performance achieved by the proposed method.

For numerical assessment of the performances of the method, the error rate measure of the extracted information is adopted. To compute the error rate, the denoised TFD is subtracted from one reference, noise-free TFD of the analyzed signal, representing the signal UIC. The total number of residual non-zero coefficients corresponds to the sum of false-positive (FP), and false-negative (FN) errors.

The reported results are based on 1000 independent realizations of additive white Gaussian noise (AWGN) for six different noise levels. The error rate is considered as a percentage of the $N \times N$-dimensional set of observations. This criterion considers both the residual noise in the extracted information (FP) and the unintentionally removed parts of the signal components (FN). The TFDs are computed by the spectrogram with *Hamming* window at each consecutive time step of N samples. The window of length W is zero-padded to N samples, being also the number of the spectrogram's frequency bins. For the results reported in this section the window is of length $W = 85$.

Insight into the performance of the proposed K-m/ICI/ICM extraction method is given in Table III. For comparison, apart from the K-m/ICI algorithm [27], results are reported for the local Rényi entropy extraction method (LRE) [26] and hard thresholding (HT) [8], [10], [14]. The K-m/ICI/ICM, K-m/ICI, and LRE, which require initial data segmentation, are computed for $K = 9$, while the HT removes all the TFD coefficients not exceeding 5% of the TFD maximum. As shown in Table III, for the reported simulation set, the K-m/ICI/ICM outperforms the other methods in 14 out of 18 trials (one trial corresponds to 1000 realizations average for a particular SNR), with the absolute prevalence of the K-m/ICI/ICM in the -6 to $0\,dB$ SNR range.

Exceptions to the general outperformance of the K-m/ICI/ICM occur for the trials *Sig1* $3\,dB$ and *Sig3* $6\,dB$, where the HT achieves best performances, improving the K-m/ICI/ICM by 27% and 25%, respectively, followed by the LRE. Yet, due to its poor adaptability, the HT underperforms on the rest of the simulation set, particularly in the lower SNR range (HT error rate improved by the K-m/ICI/ICM by up to 73%). It should be noted that differently set hard thresholds would achieve different results; however, for real data, in the lack of a reference noise-free signal, the user cannot gauge the best-performing one. The K-m/ICI/ICM and LRE perform similarly for *Sig 2* $9\,dB$, while the methods act differently in lower SNRs, with decisive prevalence of the K-m/ICI/ICM, exhibiting the most significant advantage for the trial *Sig 2* $6\,dB$ (LRE improved by 33%).

Comparison with the K-m/ICI points out the benefits of using additional information from the ICM in terms of error rate reduction. In fact, the proposed method outperforms the existing one over the entire simulation set, except for *Sig 1* $9\,dB$, where, due to negligible noise presence, the two methods achieve an equal result.

A more detailed comparison of the error distribution of the K-m/ICI/ICM and K-m/ICI is given in Fig. 8. For the three test signals, it can be observed that the proposed method almost exclusively affects the FP error component, approximately halving it in the range from low to moderate SNR. Dependency of the method performance on the number of classes K in terms of error rate, reported in Fig. 9, confirms the analysis in Section IV-A3. Larger error rate results from the extreme values of K in Fig. 9. Rough partitioning, when K is small, penalizes UIC's small coefficients, outweighing the FN error rate component. In contrast, as K increases, structural differences between classes even out, losing the criterion for their discrimination. As a result, FP estimates become the dominant error rate component. However, as visible in Fig. 9, for the tested values the span of the parameter K from 7 to 10 provides a fair trade-off between FP and FN estimates.

A final note inspects the behaviour of the proposed method with respect to signal's amplitude modulation in noisy environments.

For this purpose we consider the signal component x_n with hyperbolic FM, already reported in Fig. 4, but at this point with variable amplitude modulation, described by

$$A_n = e^{-\pi\frac{(n-N/2.5)^2}{(N/1.2)^2}}\sqrt{1-e^{-\pi\frac{(n-N/4)^2}{(N/3)^2}}-e^{-\pi\frac{(n-N/1.5)^2}{(N/3)^2}}}. \quad (34)$$

The signal x_n is embedded in AWGN, $\mathrm{SNR} = -2\,dB$. The spectrograms of the noise-free, and noisy signals are shown in Fig. 10(a), and (b), respectively. The extracted information is reported in Fig. 10(c). Figure 10(d) depicts the superimposition of UIC and extracted information supports. The extracted information support is classified as TP (violet) and FP (pink) estimates, while undesirably removed parts of the

This article has been accepted for publication in IEEE Transactions on Signal Processing. This is the author's version which has not been fully edited and content may change prior to final publication. Citation information: DOI 10.1109/TSP.2022.3223575

TABLE II: Parameters of the test signals from Fig. 7

$y_n = x_n + \nu_n$, $x_n = \sum_{l=1}^{L} A_{ln} e^{j\Phi_{ln}}$, $1 \le n \le N$, $N = 800$

		A_{ln}	Φ_{ln}
Sig1	*l=1*	$e^{-\pi \frac{(n-N/1.5)^2}{(N/2)^2}}$	$2\pi(-1.564 \cdot 10^{-4} n^2 + 0.300n - 95.093)$
	l=2	$0.75e^{-\pi \frac{(n-N/2.5)^2}{(N/2.5)^2}}$	$2\pi(9.386 \cdot 10^{-5} n^2 + 0.249n - 114.943)$
Sig2	*l=1*	$2e^{-\pi \frac{(n-N/2)^2}{(N/2)^2}}$	$0.073N \sin\left(\frac{2\pi(n-16)}{0.7N} + 1.523\right) + 0.49\pi n - 83.36$
	l=2	$2e^{-\pi \frac{(n-N/2)^2}{(N/2)^2}}$	$0.035N \sin\left(\frac{2\pi(n-18)}{0.7N} + 1.570\right) + 0.5\pi n - 0.27$
	l=3	$e^{-\pi \frac{(n-N/2)^2}{(N/2)^2}}$	$0.5\pi n - 200\pi$
Sig3	*l=1*	$\text{rect}\left(\frac{n-N/3}{N/2}\right)$	$2\pi(0.300n - 2.826 \cdot 10^{-4} n^2 + 2.352 \cdot 10^{-7} n^3)$
	l=2	$\text{rect}\left(\frac{n-N/3}{N/2}\right)$	$2\pi(0.500n - 2.826 \cdot 10^{-4} n^2 + 2.352 \cdot 10^{-7} n^3)$
	l=3	$\text{rect}\left(\frac{n-N/1.33}{N/3.2}\right)$	$2\pi(0.501n - 5.500 \cdot 10^{-4} n^2 + 3.923 \cdot 10^{-7} n^3)$
	l=4	$\text{rect}\left(\frac{n-N/1.33}{N/3.2}\right)$	$2\pi(0.250n - 4.711 \cdot 10^{-4} n^2 + 4.702 \cdot 10^{-7} n^3)$

TABLE III: Performance comparison for signals in Figs. 6 and 7. Values are averaged from 1000 simulations of the signal with different realizations of AWGN.

		Error rate [%]					
SNR [dB]		-6	-3	0	3	6	9
Sig1	K-m/ICI/ICM	**9.29**	**6.90**	**5.44**	5.65	**2.99**	**2.49**
	K-m/ICI	12.18	9.87	9.50	8.09	4.21	**2.49**
	HT	34.03	18.23	7.43	**4.10**	3.88	3.79
	LRE	11.51	9.24	6.90	4.32	3.02	2.51
Sig2	K-m/ICI/ICM	**15.94**	**13.02**	**10.10**	**7.20**	**5.70**	4.08
	K-m/ICI	18.43	15.29	11.99	8.07	9.51	4.07
	HT	39.04	25.97	13.85	7.99	7.08	7.09
	LRE	17.84	15.22	12.91	8.00	8.54	**4.01**
Sig3	K-m/ICI/ICM	**18.36**	**14.37**	**10.79**	**8.41**	9.35	**4.73**
	K-m/ICI	21.00	16.41	12.60	10.99	12.17	5.28
	HT	43.19	32.73	20.67	11.04	**7.02**	6.51
	LRE	19.74	16.36	12.70	10.49	7.51	5.14

UIC represent FN estimates (turquoise). The UIC, clearly, consists of the union of the TP and FN estimates. As visible from Fig. 10(d), loss of UIC (FN) is limited and present mostly at the margins of the signal components.

On the other hand, FP estimates are usually regions contiguous to the support of the UIC, and are thus inevitably extracted since being part of the same districts of relevant TF coefficients as signal components. Since FP peaks are not likely to appear as separated signal components, a peak-detection-and-tracking IF estimation technique [12], [47] will likely disregard them.

VI. Conclusion

We present a novel method for automatic extraction of useful information from TFDs of noisy signals. The method combines information obtained from two TF substrates of the noisy signal: the newly introduced inverse complexity map (ICM), and the energy distribution.

The ICM approach introduced in this paper gives an entropy-based insight into the TFD signal structure, consistently acting as an amplitude-invariant edge detection mechanism, while the more traditional energy distribution analysis identifies patches of higher energy content.

We find that these two approaches result in mostly disjoint TF supports, overlapping only in the proximity of the signal components. This behaviour is also a result of intrinsic structural characteristics of the TFD.

Thus, the intersection of TF substrates' supports prove reliable markers for useful information detection.

Compared to useful information extraction from the sole TF energy distribution, the proposed method exhibits a significantly reduced error rate.

Furthermore, combining the ICI and α-Rényi methods can produce a new family of entropy-based edge detection algorithms, perhaps even extensible to higher-order UIC detection.

References

[1] B. Boashash, *Time frequency signal analysis and processing: A comprehensive reference*. Elsevier Academic Press, 2016.

[2] B. Boashash, Estimating and interpreting the instantaneous frequency of a signal-part 1: Fundamentals, in Proceedings of the IEEE, vol.80, no.4, 1992, pp. 520-538, doi: 10.1109/5.135376.

[3] B. Boashash, Interpreting and estimating the instantaneous frequency of a signal-Part 2: Algorithms and Applications, in Proceedings of the IEEE, vol.80, no.4, 1992, pp.540-568, doi: 10.1109/5.135378.

[4] L. Cohen, Time-frequency distributions-a review, in Proceedings of the IEEE, vol.77, no.7, 1989, pp. 941-981, doi: 10.1109/5.30749

[5] P. Flandrin, *Time-Frequency/Time-Scale Analysis*. Academic Press, San Diego, CA, 1999.

[6] F. Hlawatsch, and G. F. Boudreaux-Bartels, Linear and quadratic time-frequency signal representation, in IEEE Signal Processing Magazine, vol.9, no.2, 1992, pp. 21-67, doi: 10.1109/79.127284.

[7] P. Flandrin, and P. Borgnat, Time-frequency energy distributions meet compressed sensing, in IEEE Transactions on Signal Processing, vol.58, no.6, 2010, pp. 2974-2982, doi:10.1109/TSP.2010.2044839.

[8] N. Linh-Trung, A. Belouchrani, K. Abed-Meraim, and B. Boashash, Separating more sources than sensors using time-frequency distributions, in EURASIP Journal on Advances in Signal Processing, vol.2005, no.17, 2005, pp. 2828–2847. https://doi.org/10.1155/ASP.2005.2828.

[9] J. Lerga, N. Saulig, R. Lerga, and I. Štajduhar, TFD thresholding in estimating the number of EEG components and the dominant IF using the short-term Rényi entropy, in Proceedings of the 10th International Symposium on Image and Signal Processing and Analysis (ISPA), Ljubljana, Slovenia, 2017, pp. 80-85.

[10] S. Stanković, and LJ. Stanković, An architecture for the realization of a system for time-frequency signal analysis, in IEEE Transaction on Circuits and Systems, Part II, no.7, 1997, pp. 600-604, doi: 10.1109/82.598433.

[11] N. Saulig, N. Pustelnik, P. Borgnat, P. Flandrin, and V. Sucic, Instantaneous counting of components in nonstationary signals, in Proceedings of European Signal Processing Conference (EUSIPCO), Marrakesh, Marocco, 2013, pp. 1-5.

[12] J. Lerga, N. Saulig, and V. Mozetič, Algorithm based on the short-term Rényi entropy and IF estimation for noisy EEG signals analysis, in Computers in Biology and Medicine, vol. 80, 2017, pp. 1-13.

[13] N. Saulig, I. Orović, and V. Sucic, Optimization of quadratic time-frequency distributions using the local Rényi entropy information, in Signal Processing - An International Journal, vol.129, 2016, pp. 17-24, doi:10.1016/j.sigpro.2016.05.025.

This article has been accepted for publication in IEEE Transactions on Signal Processing. This is the author's version which has not been fully edited and content may change prior to final publication. Citation information: DOI 10.1109/TSP.2022.3223575

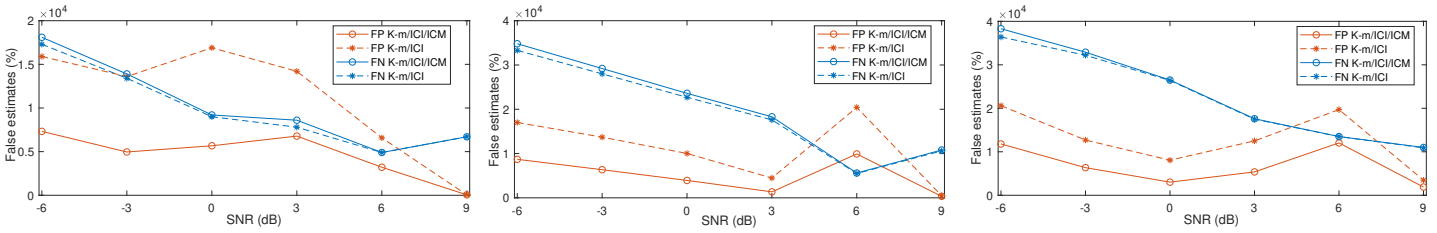

Fig. 8: Averages of false positives and false negatives across SNRs for *Sig1*, *Sig2*, and *Sig3*, respectively.

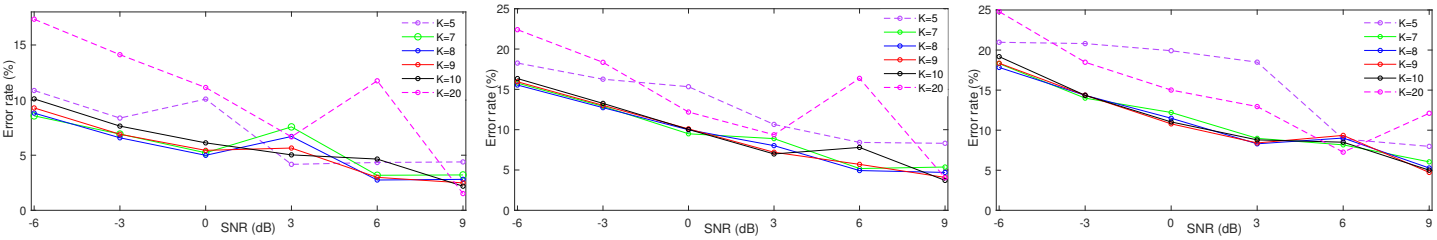

Fig. 9: Error rate for different number of classes K for *Sig1*, *Sig2*, and *Sig3*, respectively.

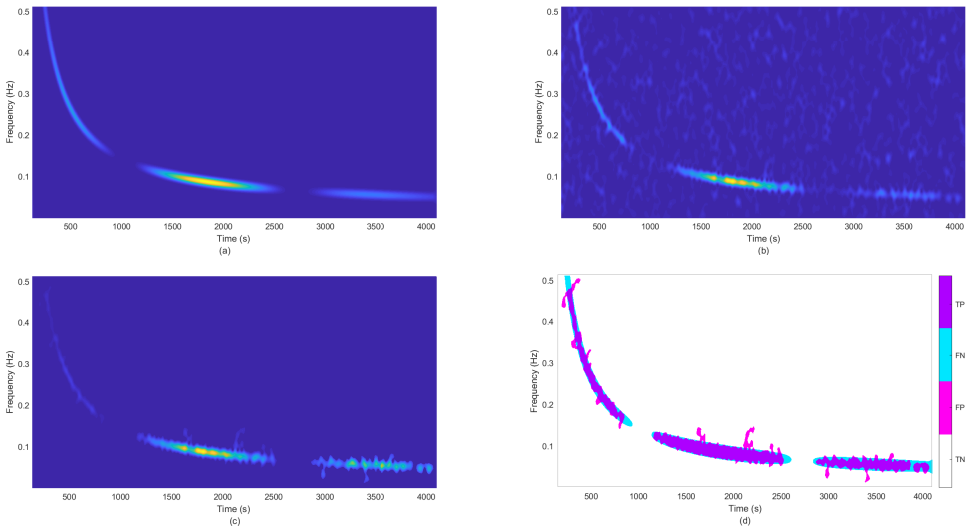

Fig. 10: Spectrogram of the noise-free signal (a). Noisy spectrogram (AWGN, $\mathrm{SNR} = -2\,dB$) (b). Information extracted by the proposed method (c). Supports of correctly classified coefficients (TP and TN), and incorrectly classified coefficients (FP and FN) (d).

[14] S. Ö. Arık, H. Jun and G. Diamos, Fast spectrogram inversion using multi-head convolutional neural networks, in IEEE Signal Processing Letters, vol.26, 2019, pp. 94-98, doi: 10.1109/LSP.2018.2880284.

[15] B. Barkat, and K. Abed-Meraim, Algorithms for blind components separation and extraction from the time-frequency distribution of their mixture, in EURASIP Journal on Advances in Signal Processing, vol.2004, no.13, 2004, pp. 2025–2033, doi: https://doi.org/10.1155/S1110865704404193.

[16] V. Bruni, M. Tartaglione, and D. Vitulano, Radon spectrogram-based approach for automatic IFs separation, in EURASIP Journal on Advances in Signal Processing, vol.13, 2020, doi:https://doi.org/10.1186/s13634-020-00673-8.

[17] F. Millioz, and N. Martin, Circularity of the STFT and spectral kurtosis for time-frequency segmentation in gaussian environment, in IEEE Transactions on Signal Processing, vol.59, no.2, 2011, pp. 515-524, doi:10.1109/TSP.2010.2081986.

[18] G. Yu, S. Mallat, and E. Bacry, Audio denoising by time-frequency block thresholding, in IEEE Transactions on Signal Processing, vol.56, no.5, 2008, pp.1830-1839, doi: 10.1109/TSP.2007.912893.

[19] H. Hassanpour, M. Mesbah, and B. Boashash, Time-frequency feature extraction of newborn EEG seizure using SVD-based techniques, in EURASIP Journal on Advances in Signal Processing, 2004, pp.2544-2554, doi:10.1155/S1110865704406167.

[20] B. Leprette, and N. Martin, Extraction of pertinent subsets from time-frequency representations for detection and recognition purposes, in Signal Processing vol. 82, 2002, pp. 229-238, doi:10.1016/S0165-1684(01)00181-5.

[21] R. Steinberg, and D. O'Shaughnessy, Segmentation of a speech spectrogram using mathematical morphology, in Proceedings of IEEE International Conference on Acoustics, Speech and Signal Processing (ICASSP), Las Vegas, Nevada, USA, 2008, pp.1637-1640, doi:10.1109/ICASSP.2008.4517940.

[22] F. Millioz, and N. Martin, Time-frequency segmentation for engine speed monitoring, Special Session on Pattern Recognition in Acoustics and Vibration, in Thirteen International Congress on Sound and Vibration, ICSV13, Vienna, Austria, July 2006.

[23] C. Meyer, and M. Spiertz, Audio segmentation using different time-frequency representations, in Proceedings of the 12th International Student Conference on Electrical Engineering, Prague, Czech Republic, May 2008.

[24] C. Tantibundhit, F. Pernkopf, and G. Kubin, Joint time-frequency segmentation algorithm for transient speech decomposition and speech enhancement, in IEEE Transactions on Audio Speech and Language Processing, vol.18, no.6, 2010, pp.1417-1428, doi:

10.1109/TASL.2009.2035037.
[25] A. Vranković, J. Lerga, and N. Saulig, A novel approach to extracting useful information from noisy TFDs using 2D local entropy measures, in EURASIP Journal on Advances in Signal Processing, vol.18, 2020, pp. 1-19, doi.org/10.1186/s13634-020-00679-2.
[26] N. Saulig, Ž. Milanović, and C. Ioana, A local entropy-based algorithm for information content extraction from time-frequency distributions of noisy signals, in Digital Signal Processing, vol.70, 2017, pp. 155-165, doi.org/10.1016/j.dsp.2017.08.005.
[27] N. Saulig, J. Lerga, Ž. Milanović, and C. Ioana, Extraction of useful information content from noisy signals based on structural affinity of clustered TFDs' coefficients, in IEEE Transactions on Signal Processing, vol.67, no.12, 2019, pp. 3154-3167, doi:10.1109/TSP.2019.2912134.
[28] W. J. Williams, M. L. Brown, and A. O. Hero, Uncertainty, information, and time-frequency distributions, in Proceedings of Advanced Signal Processing Algorithms, Architectures, and Implementations II, vol.1566, 1991, pp. 144–156, https://doi.org/10.1117/12.49818.
[29] R. G. Baraniuk, P. Flandrin, A. J. E. M. Janssen, and O. J. J. Michel, Measuring time-frequency information content using the Rényi entropies, in IEEE Transactions on Information Theory, vol.47, no.4, pp. 1391-1409, 2001, doi:10.1109/18.923723.
[30] T. D. Popescu, and T.D. Aiordăchioaie, New procedure for change detection operating on Rényi entropy with application in seismic signals processing, in Circuits Systems and Signal Processing, vol.36, no.9, 2017, pp. 3778–3798, https://doi.org/10.1007/s00034-017-0492-y.
[31] V. Sucic, N. Saulig, and B. Boashash, Estimating the number of components of a multicomponent nonstationary signal using the short-term time-frequency Rényi entropy, in EURASIP Journal on Advances in Signal Processing, vol.125, 2011, doi:125-1-125-11.
[32] I. E. Frank, and R. Todeschini, *The data analysis handbook*. Elsevier, New York, NY, 1994.
[33] V. Katkovnik, K. Egiazarian, and J. Astola, *Local Approximation Techniques in Signal and Image Processing*. SPIE Press, Bellingham, Wa, 2006, doi:10.1117/3.660178.
[34] V. Katkovnik, K. Egiazarian, and J. Astola, Adaptive window size image de-noising based on intersection of confidence intervals (ICI) rule, in Journal of Mathematical Imaging and Vision vol.16, no.3, 2002, pp. 223-235, doi:10.1023/A:1020329726980.
[35] I. Djurović, and LJ. Stanković, Modification of the ICI rule-based IF estimator for high noise environments, in IEEE Transactions on Signal Processing, vol.52 , no.9, 2004, pp. 2655-2661, doi:10.1109/TSP.2004.832030.
[36] V. Katkovnik, A new method for varying adaptive bandwidth selection, in IEEE Transactions on Signal Processing, vol.47, no.9, 1999, pp. 2567-2571, doi:10.1109/78.782208.
[37] W. Martin, and P. Flandrin, Wigner-Ville spectral analysis of nonstationary processes, in IEEE Transactions on Acoustics, Speech and Signal Processing, vol.33, no.6, 1985, pp. 1461-1470, doi:10.1109/TASSP.1985.1164760.
[38] LJ. Stanković, and V. Katkovnik, The Wigner distribution of noisy signals with adaptive time-frequency varying window, IEEE Transactions on Signal Processing, vol.47, no.4, 1999, pp. 1099-1108, doi:10.1109/78.752607.
[39] A. H. Nuttall, *Signal processing studies*. Naval Undersea Warfare Center, New London, CT, 1994.
[40] LJ. Stanković and S. Stanković, Wigner distribution of noisy signals, in IEEE Transactions on Signal Processing, vol.42, no. 2, 1993, pp. 956-960, doi:10.1109/78.193234.
[41] M. G. Amin, Minimum variance time-frequency distribution kernels for signals in additive noise, in IEEE Transaction on Signal Processing, vol.44, no.9, 1996, pp. 2352-2356, doi:10.1109/78.536695.
[42] LJ. Stanković, and V. Ivanović, Further results on the minimum variance time-frequency distribution kernels, in IEEE Transactions on Signal Processing, vol.45, no.6, 1997, pp. 1650-1655, doi:10.1109/78.600007.
[43] LJ. Stanković, *Time-frequency signal analysis: Research monograph*. Faculty of Electrical Engineering, Podgorica, Montenegro, 2004.
[44] N. Saulig, Ž. Milanović, J. Lerga and K. Griparić, On the selection of the proper number of classes in TFD segmentation for extraction of useful information content from noisy signals, in Proceedings of the 3rd International Conference on Smart and Sustainable Technologies (SpliTech), Split, Croatia, 2018, pp. 1-5.
[45] R. M. Haralick, and Shapiro L. G., *Computer and Robot Vision, Vol.1*. Addison-Wesley, Boston, MA, 1992.
[46] P. Flandrin, On detection-estimation procedures in the time-frequency plane, in Proceedings of International Conference on Acoustics, Speech and Signal Processing, 1986, Tokyo, Japan, 1986, pp. 2331-2334, doi: 10.1109/ICASSP.1986.1168669.
[47] N.A. Khan, M. Mohammadi, and S. Ali, Instantaneous frequency estimation of intersecting and close multi-component signals with varying amplitudes, in Signal, Image and Video Processing, vol.13, 2019, pp. 517–524, doi:10.1007/s11760-018-1377-7.

Nicoletta Saulig received her MS degree in Electrical Engineering from the Faculty of Engineering, University of Rijeka, Croatia, in 2009, and PhD degree in Electrical Engineering from the Faculty of Electrical Engineering and Computing, University of Zagreb, Croatia, in 2015. From 2017 she is an Assistant professor, and head of the Laboratory of Electronics at the Department of Engineering, "Juraj Dobrila" University of Pula, Croatia. She received the Silver medal "Josip Lončar" for outstanding PhD thesis from the Faculty of Electrical Engineering and Computing, University of Zagreb. Her main research interests include time-frequency signal analysis, with a particular emphasis on complexity estimation of nonstationary signals, and statistical signal analysis and processing.

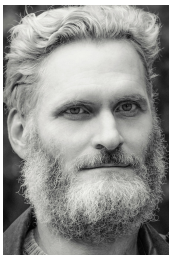

Miloš Milovanović has received MS degree in Mathematics at the University of Belgrade, Serbia in 2008 and PhD degree in Applied Mathematics at the Faculty of Technical Engineering, University of Novi Sad, Serbia in 2013. His research concerns statistical signal processing, complex systems physics and neuroaesthetics. It is supported by the Ministry of Science, Technological Development and Innovation of the Republic of Serbia through Mathematical Institute of the Serbian Academy of Sciences and Arts.

Siniša Miličić attained his PhD in Mathematics (dynamical systems and nonlinear analysis) in 2013 at the University of Zagreb, Croatia. His pure research interests include fractal analysis, dynamical systems, geometry and the interplay of mathematical physics and information theory. He is also very fond of applications of mathematics and programming, with experience in both scientific and professional software development. Siniša is an assistant professor at the Faculty of Informatics in Pula, Croatia.

Jonatan Lerga Vice Dean of the Faculty of Engineering and Head of the Center for Artificial Intelligence and Cybersecurity, University of Rijeka, Croatia, received his PhD degree from the Faculty of Electrical Engineering and Computing, University of Zagreb, Croatia, in 2011. In 2022, he received an award from the Croatian Academy of Sciences and Arts for his scientific work. His main research interests are digital signal processing, information theory, and applied artificial intelligence.